Biomedical Signal Processing and Control 31 (2017) 63–70

Contents lists available at ScienceDirect

Biomedical Signal Processing and Control

journal homepage: www.elsevier.com/locate/bspc

Fractal analysis of MR images in patients with chiari malformation: The importance of preprocessing

Engin Akar[a,*], Sadık Kara[b], Hidayet Akdemir[c], Adem Kırış[d]

[a] Department of Computer Engineering, Istanbul Gelisim University, Istanbul, Turkey
[b] Institute of Biomedical Engineering, Fatih University, Istanbul, Turkey
[c] Department of Neurosurgery, Medicana International Hospital, Istanbul, Turkey
[d] Department of Radiology, Mehmet Akif Ersoy Cardio-Thoracic Surgery Training and Research Hospital, Istanbul, Turkey

ARTICLE INFO

Article history:
Received 30 September 2015
Received in revised form 4 July 2016
Accepted 13 July 2016
Available online 21 July 2016

Keywords:
Chiari malformation
Fractal analysis
Noise filtering
Segmentation
White matter
Gray matter
Cerebrospinal fluid

ABSTRACT

As a popular method to meathe complexity of images and generally signals, FD analyses have been used in neuroimaging studies to evaluate the morphological complexity of brain structures. The aim of this study is to perform an FD-based complexity analyses of cerebellar tissues, such as cerebellar white matter (WM), cerebellar gray matter (GM) and cerebrospinal fluid (CSF) spaces around the cerebellum, on magnetic resonance (MR) images of Chiari Malformation type-I (CM-I) patients and healthy controls. Besides, to determine the noise effects on complexity of sub cerebellar structures, two common non-linear noise filters, median filter and bilateral filter, were applied to MR images and their performances were compared. Data of fourteen CM-I patients and sixteen normal subjects were used in this study. First, noise variance was estimated using a method based on skewness of the magnitude data. Second, as a preprocessing step, median and bilateral filters were applied on MR data separately to create different series of images for each filter. After the preprocessing, filtered brain images were segmented into three different tissues including WM, GM and CSF. Last, a 3D box-counting method was applied on segmented images to estimate the corresponding FD values. Our results showed that, while GM FD values was not significantly different between patients and controls ($p = 0.051$) in median filtering case, GM FD values in patients were found to be significantly lower than those in controls ($p = 0.007$) in bilateral filtering case. Additionally, in both cases, WM FD values in patients were found to be significantly lower than those in controls; however, this difference was more evident in bilateral filtering case ($p = 0.0003$) than that in median filtering case ($p = 0.013$). These outcomes indicated that bilateral filter was found to be more successful in discriminating CM-I patients from controls in cerebellar complexity analyses. In conclusion, results of this study revealed that noise removal is an important preprocessing step for a more successful analysis of digital images and bilateral filter is an effective filtering method for segmentation accuracy and FD analysis performance.

1. Introduction

Chiari Malformation type I (CM-I) is a serious neurological disorder, which was first described by Professor Hans Chiari in 1891 [1]. This condition is characterized by the downward displacement of the cerebellar tonsils, which are rounded lobule like tips of cerebellum under each of its hemisphere, into the spinal canal under the foramen magnum, which is the large opening in the base of the skull [2,3]. Radiological definition states that persons are diagnosed as having CM-I if they have a tonsillar descent of 5 mm or more below the foramen magnum [4]. Other parts of the hindbrain such as brainstem and fourth ventricle may also be affected in this disorder. They may be smaller in size or slightly deformed, however, their normal positions are not changed. Another condition associated with CM-I is syringomyelia, which is the abnormal development of a cavity that can involve a collection of cerebrospinal fluid (CSF) within the spinal cord. It may be observed in most of the CM-I patients [5].

The formation of CM-I syndrome may be triggered by several groups of conditions and disorders. These reasons include variations in the equilibrium of intracranial pressure because of altered CSF circulation dynamics [3], overcrowding of cerebellum due to small posterior fossa dimensions resulting from incomplete

* Corresponding author at: Computer Engineering, Istanbul Gelisim University, Istanbul, Turkey.
E-mail address: eakar@gelisim.edu.tr (E. Akar).

http://dx.doi.org/10.1016/j.bspc.2016.07.005
1746-8094/

development of occipital bones [6–11]. However, the actual pathogenesis and the natural history of this anomaly have not been clearly specified [6,12]. CM-I patients may show several symptoms with different severity degrees. The most frequent symptom is severe headaches at the back of the head, which may result from the head movements such as coughing, laughing and sneezing. Another common symptom is the pain in shoulders and in the neck [13,14]. Additionally, a group of less frequent symptoms include sleep apnea [15,16]; nystagmus, which is a neurological condition involving rapid involuntary eye movements [17]; balance and gait problems [18] and dysarthria, which is a motor speech disorder causing disruption of speech quality [19]. Interestingly, some patients may not show any symptom, even though they have a tonsillar descent of more than 5 mm [20].

Midline magnetic resonance imaging (MRI) slices provide a suitable view of cerebellar tonsils; therefore, MRI is the preferred modality for the diagnosis of CM-I [21]. Besides, neurological tests, computed tomography (CT), and phase contrast (PC) cine MRI are additional diagnostic methods, which are used for the identification of this anomaly and for attainment of necessary information to make a suitable treatment plan as well [6,22–24]. Surgical operations are the only therapeutic methods to improve the conditions of patients. These operations, which are generally referred as posterior fossa decompression (PFD) [25], are aimed to restore CSF flow blockage between the brain and the spinal canal [26,27] or to enlarge the posterior cranial fossa (PCF).

Previous MRI studies related to CM-I research mainly dealt with morphological assessment of hindbrain structures such as cerebellum, fourth ventricle, PCF, brainstem and entire brain as well [6,8–10,28,29]. Several linear and volumetric analyses were carried out using sagittal MRI slices to evaluate the structural features of PCF. An essential measurement is the determination of the length of cerebellar tonsils under foramen magnum. Additionally, measurements related to occipital bones including lengths of clivus and supraocciput and calculation of the slope of tentorium were performed for linear analysis of PCF [6]. Furthermore, several volumetric assessment of this syndrome were also carried out using total volume of brain, PCF and CSF regions [6,8–10,28,29]. All these studies were related to size of the brain tissues and bone parts that surrounds it. To investigate the variations in inner structures of cerebellar tissues in CM-I patients, we have performed a 2D fractal analysis of cerebellum after segmenting it into white matter (WM), gray matter (GM) and CSF using a single sagittal MRI slice [30]. On the other hand, evaluation of CSF flow characteristics were also performed to determine the relation between CM-I symptoms and CSF flow patterns and to distinguish symptomatic cases of this disorder from asymptomatic cases [31–33].

A popular method for performing quantitative evaluation of morphological complexity is fractal dimension (FD) analysis [34–42]. A numerical value is generated by this method to process the structural details in complex objects [34–36]. FD analysis was used in a broad category of studies in neuroscience such as evaluation of the morphology of the brain cortices in neurological disorders [37], structural and functional changes in complexity of neural system during development or degeneration of brain [35,38–40]. Therefore, this analysis was applied in many neurological disorders such as multiple sclerosis (MS) [35,41], schizophrenia [34], Alzheimer's disease [42], multiple system atrophy [36], obsessive-compulsive disorder [34] and CM-I [30].

Accurate segmentation of brain tissues that includes complex structures in various neurological disorders such as CM-I is considered as an important step for the diagnosis. In previous studies, it has been reported that there are difficulties in finding edges or boundaries between different regions in MRI images, which have small intensity variations among pixels [43,44]. Another important problem in image analysis is segmentation of noisy images. Particularly, to classify three main brain structures, such as WM, GM, and CSF, intensity-based segmentation algorithms, that divide each pixels/voxels based on their intensity, are used. In the intensity-based segmentation, the intensity values of brain tissues in MRI images are modeled by a mixture of Gaussian and Rician probability distribution functions [45]. However, it has been reported that these types of segmentation require some tools for artifact elimination such as noise [46]. Because MRI images include various sources of noise, such as salt and pepper noise, speckle noise, Gaussian noise and Rician noise; these types of artifacts must be removed from MR data using filters to decrease misclassification problems and unrealistic results [44]. Therefore, in some of the previous studies on other neurological disorders such as MS, extensive pre-processing algorithms have been implemented on MRI data for noise removal [47].

The main purpose of the present study is to determine the effects of pre-processing on FD analysis of sub-cerebellar tissues in MRI data obtained from CM-I patients. To this end, two common nonlinear filters, median and bilateral filters, were employed and compared. The effects of denoising were evaluated using the results of FD analyses on WM, GM, and CSF, respectively. To our knowledge, no study has yet analyzed and compared the effects of pre-processing on FD analysis results of MRI. Thus, this research represents one of the first studies that investigate the effect of applying different noise filtering techniques on structural complexity analysis of MRI data from CM-I patients and healthy controls to achieve better statistical results.

2. Material and methods

2.1. MRI data

Brain MR images of 15 CM-I patients (4 males and 11 females, 16–55 years age range) and 16 healthy subjects (5 males and 10 females, 16–50 years age range) were obtained from databases of the radiology departments of two hospitals: Mehmet Akif Ersoy Cardio-Thoracic Surgery Training and Research Hospital and Medicana International Hospital, Istanbul. These data, which were taken in the period between 2013 and 2015, were selected from already existing MRI records at the hospitals mentioned above. The experimental procedures of this study were approved by the Ethical Committee of Fatih University. Three-dimensional high-resolution MRI data were recorded using a Siemens Symphony Magnetom Aera 1.5 T MR scanner (Erlangen, Germany). MR image parameters include: A matrix size of 512×512 pixels and in-plane resolution of 0.5 mm × 0.5 mm, flip angle 90°, TE (echo time) 9.8 ms, TR(repetition time) 511 ms, FOV 25 cm, 24 contiguous 5 mm sagittal slices.

2.2. Noise characteristics of MRI

Thermal effects originated from the stochastic motion of free electrons are a major noise source in MRI. This noise can be assumed to be white, additive and described by a Gaussian distribution with an equal variance and zero mean [48]. The real and imaginary components of an MR image are reconstructed applying Fourier transformation to the acquired raw complex MR data. Since the Fourier transform has linearity and orthogonality principles, the data in real and imaginary parts continue to follow Gaussian distribution [49]. Magnitude values are obtained for each pixel by calculating square root of the sum of two independent random variables from the real and the imaginary images to produce the Magnitude image. The noise features of the obtained magnitude

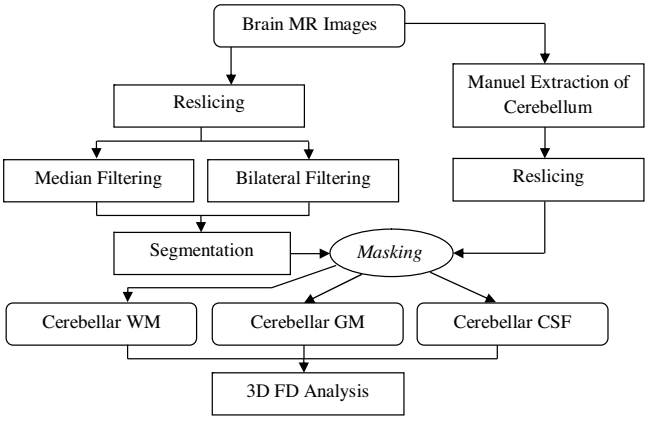

Fig. 1. Steps of image processing.

image follows a Rician distribution [50] and the corresponding probability distribution function (PDF) is described by [51]

$$P_{Mag}(M) = \frac{M}{\sigma^2} e^{-\frac{M^2+A^2}{2\sigma^2}} I_0\left(\frac{A.M}{\sigma^2}\right) \quad (1)$$

where I_0 is the modified first kind Bessel function of order zero. $M = \sqrt{\mathcal{R}^2 + \mathcal{S}^2}$ is the measured pixel intensity and $A = \sqrt{\mu_{\mathcal{R}}{}^2 + \mu_{\mathcal{S}}{}^2}$. is the image pixel intensity that does not contain noise. $\mathcal{R}$ and $\mathcal{S}$ are the real and imaginary components of the complex MR data that contain zero mean Gaussian noise with the standard deviation σ. Signal-to-noise ratio (SNR), which is characterized by the ratio $\frac{A}{\sigma}$, affects the shape of Rician distribution. When SNR value is close to zero, the Rayleigh distribution, a special case of Rician distribution, is obtained. Its PDF is given below:

$$P_{Mag}(M) = \frac{M}{\sigma^2} e^{-\frac{M^2}{2\sigma^2}} \quad (2)$$

On the other hand, when SNR is large, Rician distribution shows Gaussian distribution properties with the following PDF:

$$P_{Mag}(M) = \frac{1}{\sqrt{2\pi\sigma^2}} e^{-\left(M-\sqrt{A^2+\sigma^2}\right)/2\sigma^2} \quad (3)$$

2.3. Study procedure

The present study aims to show the significance of image preprocessing by comparing the results of complexity analysis on brain MR images which were filtered by two different denoising methods: standard 2D median filtering and bilateral filtering. The operational steps that were implemented in this study are summarized in Fig. 1. The image processing tasks in this study were implemented in three major phases. First, using MATLAB based functions and a graphical user interface application developed in MATLAB environment, the cerebellum and the surrounding CSF regions were extracted manually from the entire brain image. The image slices containing the extracted parts were resliced to achieve an isotropic resolution of $1 \times 1 \times 1\,\text{mm}^3$. After that, the binary mask files were generated using the resliced images. Second, the MR images that contained the entire brain resliced to get the isotropic resolution $1\,\text{mm}^3$ in a similar way as described in the first phase. At this stage, the resliced image files were filtered using two different noise filtering methods. One of them was the standard 2D median filtering method with default parameters and the other method was Bilateral filtering. These denoising operations generated two different filtered MR image series. After this point, the same tasks were performed on both filtered image series. The initial task that was applied on both series was an automatic segmentation to separate the brain into different cluster of tissues including WM, GM and CSF. This segmentation operation were fulfilled using the methods provided by SPM12 (Statistical Parametric Mapping) software package. Afterward, the segmented images were masked using the binary mask image series that was created in the first phase. Masking operation yielded the final segmented image series that contained the cerebellar WM, GM and CSF spaces around the cerebellum (Fig. 2). In the third and final phase, fractal dimension values were calculated for the three segmented image series using a 3D box-count algorithm to implement a complexity analysis to specify the variations between patients with CM-I and healthy controls.

2.4. Noise estimation and preprocessing

Noise variance provides a measure to quantify the quality of the MR image data and it is an important parameter for the subsequent image processing tasks such as noise filtering, clustering and segmentation [52,53]. In this study, noise variance of the MR images was calculated using an approach that is based on a local skewness computation of the magnitude data distribution. The details of this method can be found in [54]. Estimated noise variance was used to determine the intensity weight factor of bilateral filtering method.

2.4.1. Median filtering

Median Filtering suggested by Tukey [55], is a popular and widely used nonlinear method to remove the noise from images. This filter iterates over an entire image pixel by pixel and replaces a pixel value with the median value of pixels located in its neighborhood. More specifically, the algorithm of median filtering can be described as follows. Let $\left[I_{ij}\right]$ be a matrix that represents a digital image. The output of median filtering in an m by n window, where m and n are odd integers, is another image $[\bar{I}_{ij}]$. A pixel element p_{ij} in the output image is equal to the median value of intensity values of pixel elements located in an mxn neighboring window of a pixel p_{ij} in the input image. In this study, standard 2D median filtering with default parameters of windows size (3x3) was applied to each MR image slice.

2.4.2. Bilateral filtering

Bilateral filter is a simple, non-iterative and nonlinear filter, which was developed by Tomasi and Manduchi [56], for removing noise while keeping important features of images, such as edges. Traditional filters perform filtering process in the domain of an image. In other words, they take into account the geometric closeness of pixels as a weighing factor. However, bilateral filter combines this approach with a filtering in the range of an image. In this second approach, pixel values of an image are averaged with weight parameters that depend on the radiometric distance between them. Since image intensity affects the weighing parameters, range filtering is considered to be non-linear [57,58]. The product of the domain filter and the range filter components compose the expression of bilateral filter in each neighborhood. Bilateral filter calculation for a pixel located at x is performed using the following formula [59]

$$\bar{I}(x) = \frac{1}{C} \sum_{y \in N(x)} e^{\frac{-y-x^2}{2\sigma_d^2}} e^{\frac{-|I(y)-I(x)|^2}{2\sigma_r^2}} I(y) \quad (4)$$

where $N(x)$ indicates the spatial neighborhood around x, y represents the location in the neighborhood, σ_d and σ_r are control parameters to arrange the decay of the weight factors in spatial

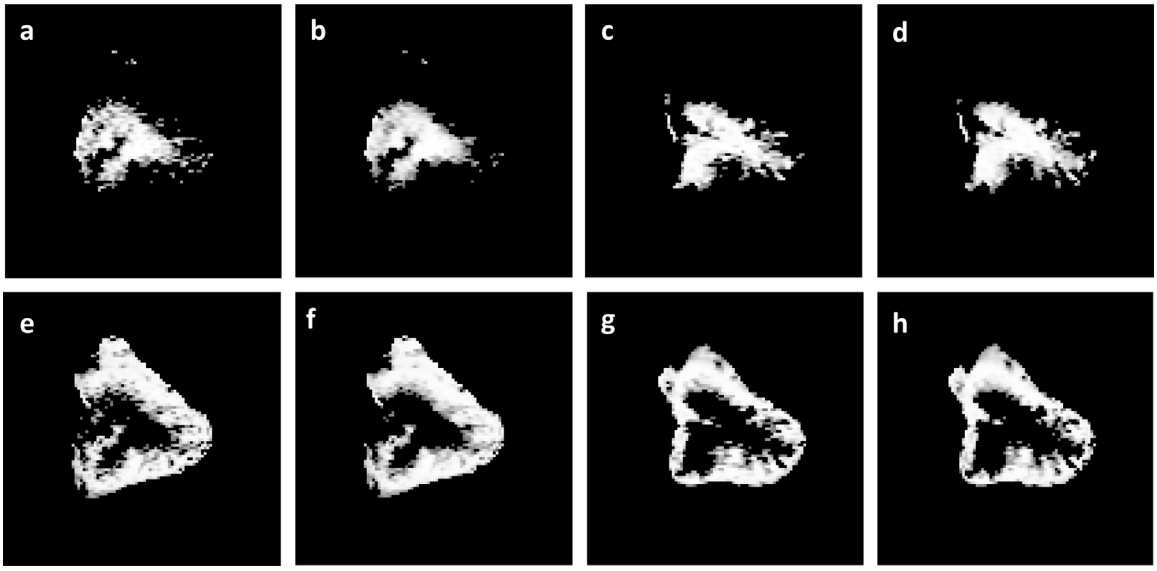

Fig. 2. Segmented images of cerebellum after median and bilateral filtering method. Cerebellar WM tissue of a patient segmented after a) median filtering, b) bilateral filtering. WM tissue of a healthy control segmented after c) median filtering, d) bilateral filtering. Cerebellar GM tissue of a patient segmented after e) median filtering, f) bilateral filtering. GM tissue of a control segmented after g) median filtering, h) bilateral filtering.

and intensity domains, respectively. In this formula, C is the normalization constant, which is given by,

$$C = \sum_{y \in N(x)} e^{\frac{-y-x^2}{2\sigma_d^2}} e^{\frac{-|I(y)-I(x)|^2}{2\sigma_r^2}} \quad (5)$$

In this study, window size parameter of bilateral filter (size of (x)) was set to $11x11$. Riji et al. suggested 1.8 for the spatial domain weight factor control parameter (σ_d), therefore, in the present work, $\sigma_d = 1.8$ was accepted as the second parameter. The final parameter (σ_r) was selected according to the estimated noise level of original MR image. To determine a suitable value for σ_r, some preliminary experiments were conducted. Based on the results of this experiments, $\sigma_r = \sigma \times 2$ were used, where σ was the estimated noise variance of the MR image to be filtered.

2.5. Fractal analysis

FD values were used to perform complexity analyses of cerebellar WM, GM and CSF spaces around the cerebellum. A 3D box-counting method, which was developed as custom software in MATLAB as extension of 2D box-counting approach, was employed in this study to estimate the FD values of mentioned structures. Many studies used this technique previously, since it is robust, easy to implement and applicable on objects like brain structures, which have a certain scale of self similarity [60].

3D box-counting method can be implemented as follows. First, a volumetric image of interest is covered by a grid of boxes. Then the boxes that contain at least one voxel having an intensity value greater than zero are counted. This process continues iteratively and in each iteration, the box size value is incremented. In this study, the iterations were initiated with a box size of 2 and the loop was executed while the box size value was less than one third of the smallest dimension of the image. A 3D visualization of box counting approach is demonstrated in Fig. 3. When the counting of non-empty boxes for each possible box size value is finished, the FD value can be estimated using the following equation [61].

$$\ln(Nr) = \mathrm{FD} \ln\left(r^{-1}\right) + \ln(\mathrm{K}) \quad (6)$$

where $Nr$is the number of boxes containing at least one voxel having an intensity value greater than zero, FD denotes the box-counting fractal value of the corresponding image, and K is any constant value.

Since the brain images are not pure fractals, determining an appropriate box-size range is essential [60]. If the selected box-size to cover an image of interest is too small or too large, the FD value of that image cannot be estimated properly [62]. Accurate estimation of FD value requires the linear part of the equation given in (6). Therefore, whole data set was evaluated using a linear regression analysis that is shown in Fig. 4a. Correlation coefficients of different line segments were checked and the slope of the segment having the highest correlation coefficient was accepted as the FD value of the image of interest. The validity of our algorithm was checked using a Menger cube of size $243 \times 243 \times 243$ (Fig. 4b), which was generated using MATLAB. FD calculation program produced 2.7289 for the generated Menger cube which is a proximate value to its theoretical FD value of 2.726833 (log20/log3).

Table 1
Demographic data of subjects and study results.

	Patients		Controls		p-value	
Gender (M/F)	4/10		5/11		–	
Age	38.93 ± 12.66		36.75 ± 6.04		0.504	
	Median	BF	Median	BF	Median	BF
WMFD Value	2.20 ± 0.08	2.14 ± 0.13	2.26 ± 0.05	2.28 ± 0.05	0.013	0.0003
GMFD Value	2.46 ± 0.05	2.45 ± 0.05	2.49 ± 0.04	2.50 ± 0.04	0.051	0.007
CSF FD Value	2.23 ± 0.08	2.23 ± 0.11	2.34 ± 0.07	2.35 ± 0.08	0.0004	0,001

M/F: male/female, WM FD Value: FD value of cerebellar white matter, WM FD Value: FD value of cerebellar gray matter, CSF FD Value: FD value of cerebrospinal fluid surrounding the cerebellum.

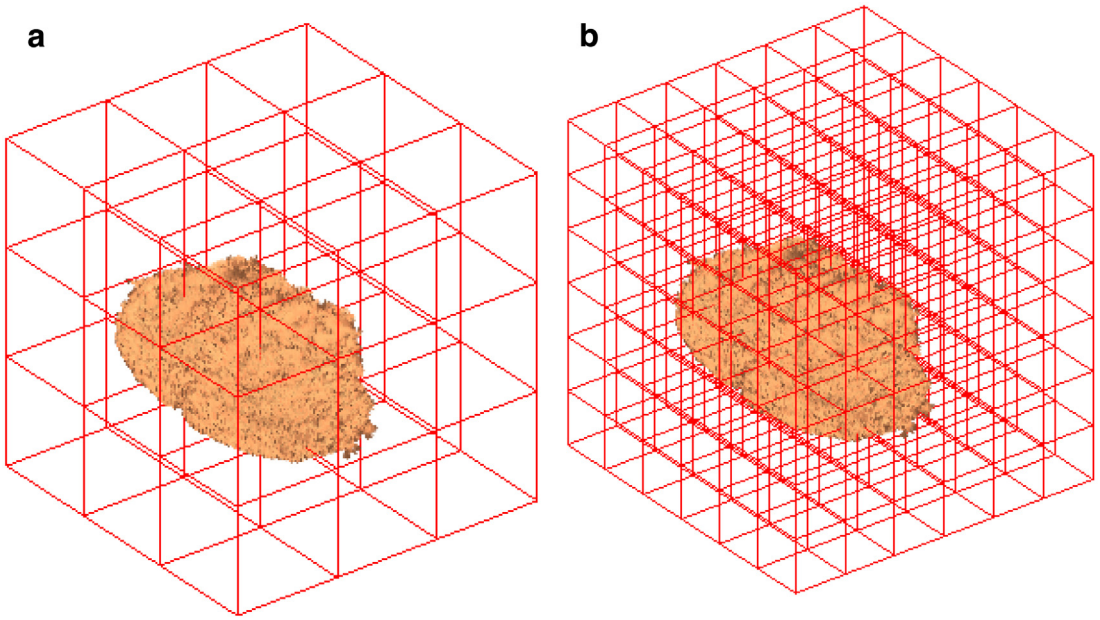

Fig. 3. Graphical illustration of a 3D box-counting method. Image of cerebellum is mapped into a grid of cubes of size (a) 20 pixels, and (b) 10 pixels (edge length).

2.6. Statistical analysis

Independent samples *t*-test was used to evaluate the variations in FD values of cerebellar tissues WM and GM and CSF spaces around the cerebellum between healthy control subjects and patients with CM-I. A Kolmogorov-Smirnov test was employed to check the normality of data showing that no significant differences were found in the cerebellar features between patients and controls. SPSS version 20.0 (SPSS Inc., Chicago, Illinois) were used for all the statistical analyses. The significance level ($p < 0.05$) was chosen for all results.

3. Results

In this study, performances of two different noise elimination methods, median filtering and bilateral filtering, were compared using the results of FD value analysis on cerebellar WM, GM and CSF regions around the cerebellum. The numerical and statistical results of this analysis are listed in Table 1. The mean FD value for cerebellar WM was found to be 2.20 for patients with a standard deviation value of 0.08 after a median filtering was applied to the source MR image files. The corresponding mean and standard deviation values for controls after a median filtering were 2.26 and 0.05, respectively. On the other hand, after a prior application of bilateral filtering noise removal method, the FD value results for cerebellar WM for patients and controls were changed as follows. The mean and standard deviation values for patients were found to be 2.14 and 0.13, respectively. Additionally, the mean FD results for controls in this second approach were 2.28 with a standard deviation of 0.05. The statistical significance between the results in median filtering case was $p = 0.013$. On the other hand, *p*-value was found

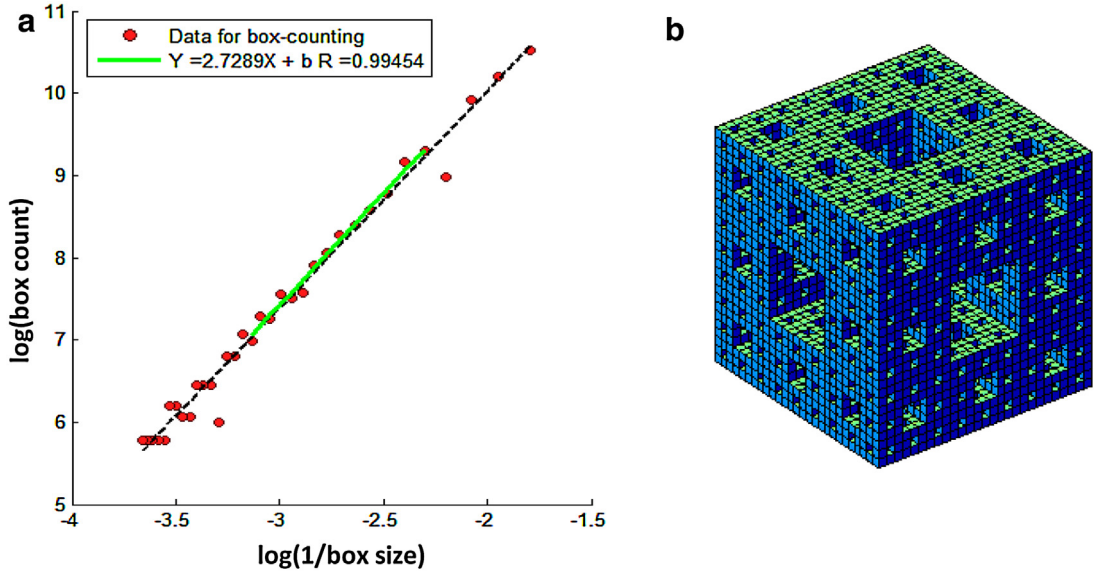

Fig. 4. A proper fractal dimension value is estimated by means of a regression analysis. a) A sample chart for a regression line. b) Artificially generated Menger cube of size $243 \times 243 \times 243$ voxels to validate the results.

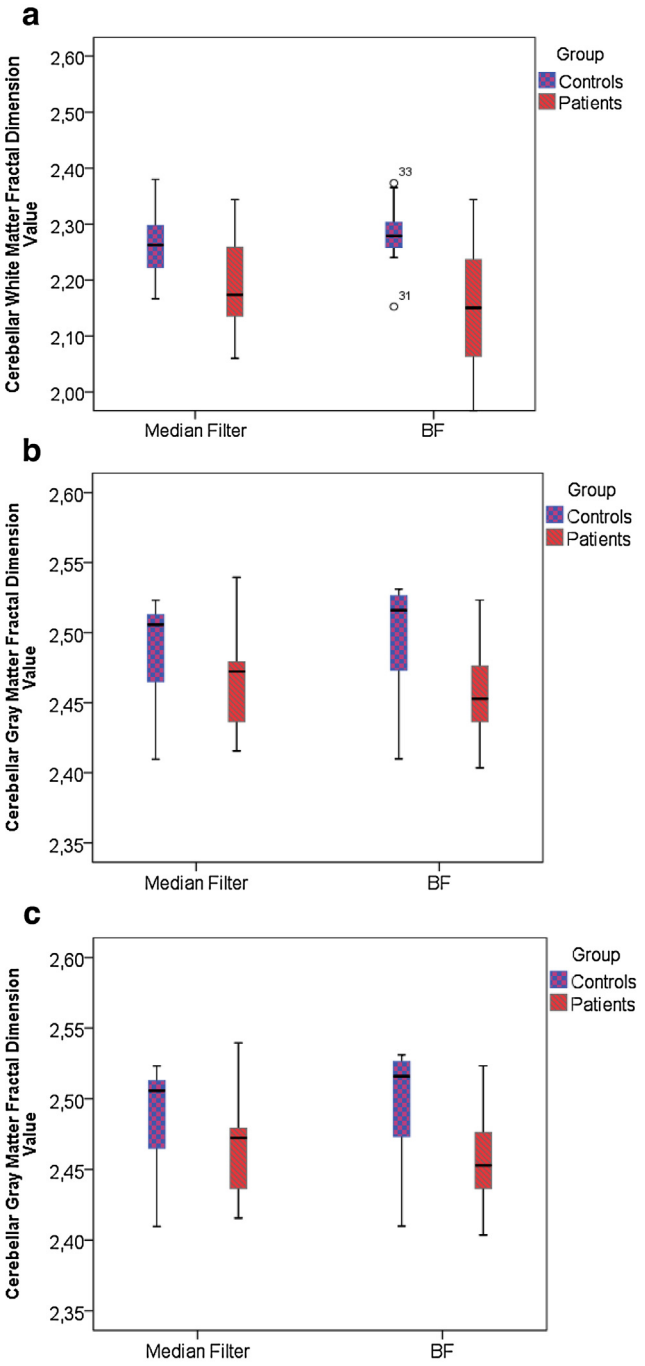

Fig. 5. Box-plot diagram of FD value results for patients and controls after a prior application of median and bilateral filtering. FD value differences of a) cerebellar WM, b) cerebellar GM and c) CSF around the cerebellum between patients and controls categorized by median and bilateral filtering methods.

to be 0.0003 in bilateral filter case. This condition is illustrated in box-plot diagram displayed in Fig. 5a.

The results of cerebellar GM FD value estimation for patients, after prior noise elimination by median filtering, were 2.46 and 0.05 as mean and standard deviation values, respectively. The corresponding results for controls after the same noise filtering process were 2.49 and 0.04. The difference between these results were not found to be statistically significant ($p = 0.051$). Different results were found when the prior noise elimination methods were changed. When a bilateral filter was applied for removing noise, FD estimation procedure yielded the numbers: 2.45 and 0.05 for patients and additionally 2.50 and 0.04 for controls. Unlike the statistical results of median filtering case, the statistical difference between FD complexity values in the bilateral filtering case were strongly significant ($p = 0.007$). Box-plot diagram in Fig. 5b displays these results categorized by median and bilateral filtering approaches.

CSF FD value results for both groups are displayed in Fig. 5c. The mean and the standard deviation values of CSF FD for patients were found to be 2.23 and 0.08. Besides, 2.34 and 0.07 were the results of CSF FD estimation for controls. These values were calculated from segmented images after a prior median filtering was performed for denoising. Statistical analysis showed that there was a significant difference between the results of patients and controls ($p = 0.0004$). Additionally, FD values were also calculated from CSF images which had been segmented from MR image slices filtered by bilateral filter previously. These values include 2.23 and 0.11 for patients and 2.35 and 0.08 for controls. In this case, the statistical difference between patients and controls was also significant ($p = 0.001$).

4. Discussion and conclusion

This paper investigates the effects of two noise elimination techniques (median filtering and bilateral filtering) on complexity analyses of sub-cerebellar tissues in CM-I patients and controls to understand the importance of preprocessing in MRI data analysis. Complexity analyses on WM, GM and CSF spaces around the cerebellum were performed using FD values, which were estimated by employing a 3D box-counting method, to assess morphological complexities in these sub-regions. To our knowledge, this is the first study investigating preprocessing effects in MRI-based cerebellar complexities in CM-I patients. FD analysis is an appropriate method for evaluating morphological features in objects, since FD is an indicator for morphological complexity. It has been suggested that an increase in FD values may imply a more complex structure, conversely, lower FD values may indicate a deterioration in object structure [35].

Diagnosis of CM-I can be performed using sagittal MR images of brain [21]. The main criterion is the length of cerebellar tonsils under the foramen magnum. If the descent of the tonsils is 5 mm or more, the patient is diagnosed as CM-I [4]. However, there are contradictory conditions in which, some patients having a tonsillar descent of far more than 5 mm in length, do not show any symptoms while some others [20], which own tonsillar descent of size less than 5 mm, may have severe symptoms of the disease [6]. Therefore, using the size of cerebellar tonsils' herniation as the primary criterion may not be enough for a successful diagnosis of this anomaly [19,23]. Investigating the morphological properties of different regions in MRI data may contribute the identification process of this disorder. It was reported that FD analysis is a suitable approach for structural complexity in objects [63]. It was further suggested that FD provides a single numerical value for the evaluation of brain cortex morphology and variations in the FD value may be an indication of cortex abnormalities [38]. Therefore, this study employed FD analysis on cerebellar tissues to support the diagnosis process of CM-I in patients.

First of all, results of our study showed that FD values for cerebellar GM values in CM-I patients have been found to be lower than those in healthy controls. Similarly in a previous study, Wu et al. [36] reported that GM tissue in patients with multiple system atrophy of the cerebellar type exhibited significantly lower FD values representing lower morphological complexity. Moreover, the decreased FD values in GM of brain and cerebellum have been reported to be related to degeneration or damage in this tissue [36]. Therefore, reduced FD values indicate that patients' GM tissues are structurally more irregular. It must be taken into account that this

difference between patients and controls was found to be nearly significant when a prior median filter was applied to MRI data ($p = 0.051$). However, it was found to be highly significant when the bilateral filter was used for preprocessing ($p = 0.007$). Second, we found that patients had significantly lower FD values than control subjects in cerebellar WM when both median filter ($p = 0.013$) and bilateral filter ($p = 0.0003$) were applied to MRI images for noise elimination. In other words, the observed difference in FD values of cerebellar WM between two groups became more significant after a bilateral filter application instead of a median filtering in MRI analysis. Therefore, the observed differences between two groups in terms of FD values may change depending on pre-applied noise filtering technique. This is in line with the findings of past studies [43,44,64–72] stating that noise removal in MRI data is an essential task for image analysis. It has been reported that the noise in medical images may restrict the visual investigation for clinicians and may cause obtaining unreliable results from image processing tasks such as segmentation [43]. Specifically, segmentation of brain MRI images is a challenging task because of the low contrast in differentiating certain brain regions. It is difficult to find out the boundaries between different regions because of very small intensity variation between pixels. For this reason, to improve the segmentation accuracy, removing noise from images is reported to be very crucial [44]. However, in most of the segmentation or other MRI image analysis studies, median filters have been used for preprocessing [44,64–67]. Additionally, some of the other studies compared the performance of some linear, nonlinear or transform domain filters in MRI data [43,68–72]. Nevertheless, a comprehensive study that investigates the effects of noise filtering on the complexity analysis is missing.

FD value represents the extent that an object fills space. Different from the standard Euclidian geometry which classifies smooth geometrical shapes with integer dimension values, the fractal geometry classifies complex structures with non-integer dimension values [63]. Accurate representation of an object is crucial in correct estimation of FD values. We believe that the prior application of an edge preserving noise filtering approach such as bilateral filtering contributes to correctness of the segmentation process of an interested region, therefore FD calculations after the segmentation may produce more reliable results.

In previous studies, additional algorithms were proposed as edge preserving noise removal approaches including non-local means, anisotropic diffusion, wavelet thresholding [73] and total variation filtering [74]. Using these techniques may affect the results of following FD calculations as they may change the segmentation outcome. Several techniques were proposed to calculate the FD values of objects such as methods to calculate Hausdorff, Minkowsky, box counting and mass-radius dimensions. Box counting method, which was employed in the present study, is suitable for estimating the FD of biological structures in 2D and 3D. Other mentioned approaches are useful in neuroscience applications [63]. Using different FD calculation methods may be another factor to affect the results of this study.

In the present study, resampling of images into 1 mm^3 voxel size were achieved using linear interpolation. Various approaches such as nearest neighbor, quadratic, B-Spline, cubic, Lagrange and Gaussian interpolation [75] were proposed in the literature to resample the images. Using different interpolation methods may implicitly change the FD results since the quality of resampled images depends on the applied interpolation technique. Another factor that may affect the results of this study is the segmentation method that can be used to obtain cerebellar tissues such as WM and GM. This study employed SPM based functions for the automatic segmentation of these tissues.

Although FD is performed in some studies with non-medical image analysis, it has been reported that there is no information about the noise effects on estimation of FD values [76]. Our results confirm that bilateral filtering approach successfully eliminates the noise considering Rician characteristics and preserves important image feature such as edges than the median filtering approach. One possible explanation to this result is the effects of median operation itself. In some previous studies, median filters have been reported to have some drawbacks, such as erasing fine details and rounding the corners [66,77]. Therefore, the observed low differences in FD values between patients and controls when the median filter was applied may be related to these known unwanted characteristics of median filtering.

To conclude, this study compared the performances of two popular nonlinear filter for noise elimination, median filtering and bilateral filtering, using FD analyses of cerebellar tissues such as WM, GM and CSF regions around the cerebellum. Our results showed that FD analyses with bilateral filter approach was more successful in discriminating the CM-I patients and controls than median filtering. These results further suggest that preprocessing of digital images is essential for post-processing tasks such as segmentation and morphological analysis. Nevertheless, future works are also needed to confirm the results of this study. This study should be performed on groups having large population numbers. In addition, It may be better to compare the results of this study with the performance of other denoising approaches such as anisotropic diffusion, non-local means and total variation in the future studies. Moreover, to highlight the importance of preprocessing on the FD values, the study can be extended with the results when no preprocessing step is applied before the segmentation operations.

Acknowledgements

This research was supported by the Fatih University Research and Development Management Office under project number P58011501_B.

References

[1] H. Chiari, Über Veränderungen des Kleinhirns in folge von Hydrocephalie des Grosshirns (in german), Dtsch. Med. Wschr. 17 (1891) 1172–1175.
[2] G.K. Bejjani, Definition of the adult Chiari malformation: a brief historical overview, Neurosurg. Focus 11 (2001).
[3] C. Cai, W.J. Oakes, Hindbrain herniation syndromes: the Chiari malformations (I and II), Semin. Pediatr. Neurol. 4 (3) (1997) 179–191.
[4] A.D. Elster, M.Y.M. Chen, Chiari I malformations: clinical and radiologic reappraisal, Radiology 183 (1992) 347–353.
[5] A.G. Osborn, Disorders of Neural Tube Closure. In Diagnostic Neuroradiology, ed. 2, Mosby, St. Louis, 1994, p. 15.
[6] T.H. Milhorat, M.W. Chou, E.M. Trinidad, R.W. Kula, M. Mandell, C. Wolpert, M.C. Speer, Chiari I malformation redefined: clinical and radiographic findings for 364 symptomatic patients, Congr. Neurol. Surg. 44 (5) (1999) 1005–1017.
[7] T.H. Milhorat, M. Nishikawa, R.W. Kula, Y.D. Dlugacz, Mechanisms of cerebellar tonsil herniation in patients with Chiari malformations as guide to clinical management, Acta Neurochir. (Wien) 152 (7) (2010) 1117–1127.
[8] B. Badie, D. Mendoza, U. Batzdorf, Posterior fossa volume and response to suboccipital decompression with Chiari I malformation, Neurosurgery 37 (1995) 214–218.
[9] M. Nishikawa, H. Sakamoto, A. Hakuba, N. Nakanishi, Y. Inoue, Pathogenesis of Chiari malformation: a morphometric study of the posterior cranial fossa, J. Neurosurg. 86 (1997) 40–47.
[10] H. Nyland, K.G. Krogness, Size of posterior fossa in Chiari type 1 malformation in adults, Acta Neurochir. 40 (1978) 233–242.
[11] L.J. Stovner, U. Bergan, G. Nilsen, O. Sjaastad, Posterior cranial fossa dimensions in the Chiari I malformation: relation to pathogenesis and clinical presentation, Neuroradiology 35 (1993) 113–118.
[12] F. Novegno, M. Caldarelli, A. Massa, D. Chieffo, L. Massimi, B. Pettorini, G. Tamburrini, C. Di Rocco, The natural history of the Chiari type I anomaly, J. Neurosurg. Pediatr. 2 (2008) 179–187.
[13] A.A. Talal, O.M. el-Shmam, Chiari malformation type I: a new MRI classification, Magn. Reson. Imaging 15 (4) (1997) 397–403.
[14] Carlson M.D., Muraszko M.K., 2003. Chiari I Malformation With Syrinx Pediatric Neurology. Volume 29, Issue 2, Pages 167–169.
[15] B. Lam, C.F. Ryan, Arnold-Chiari malformation presenting as sleep apnea syndrome, Sleep Med. 1 (2000) 139–144.

[16] T. Kitamura, S. Miyazaki, H. Kadotani, T. Kanemura, M. Okawa, T. Tanaka, I. Komada, T. Hatano, H. Suzuki, Type I Chiari malformation presenting central sleep apnea, Auris Nasus Larynx 41 (2) (2014) 222–224.
[17] C. Pieh, I. Gottlob, Arnold-Chiari malformation and nystagmus of skew, J. Neurol. Neurosurg. Psychiatry 69 (2000) 124–126.
[18] M.D. Staudt, Gait disturbances and seizure-like episodes in a patient with a Chiari malformation, UWOMJ 81 (Issue S1) (2013), Summer Supplement.
[19] R. Yassari, D. Frim, Evaluation and management of the Chiari malformation type 1 for the primary care pediatrician, Pediatr. Clin. North Am. 51 (2) (2004) 477–490.
[20] J. Meadows, M. Kraut, M. Guarnieri, R.I. Haroun, B.S. Carson, Asymptomatic Chiari type I malformations identified on magnetic resonance imaging, J. Neurosurg. 92 (2000) 920–926.
[21] A. Cama, P. Tortori-Donati, G.L. Piatelli, et al., Chiari complex in children—neuroradiological diagnosis, neurosurgical treatment and proposal of a new classification (312 cases), Eur. J. Pediatr. Surg. (suppl. 1) (1995) 35–38.
[22] P.R. Choudhury, P. Sarda, P. Baruah, S. Singh, A magnetic resonance imaging study of congenital Chiari malformations, OA Case Rep. 2 (8) (2013) 73.
[23] A.A. Khan, S.N. Bhatti, G. Khan, E. Ahmed, A. Aurangzeb, A. Ali, A. Khan, S. Afzal, Clinical and radiological findings in Arnold Chiari malformation, J. Ayub Med. Coll. Abbottabad 22 (2) (2010) 75–78.
[24] V.M. Haughton, B.J. Iskandar, Measuring CSF flow in Chiari I malformations, Neuroradiol J. 19 (2006) 427–432.
[25] R. Navarro, G. Olavarria, R. Seshadri, G. Gonzales-Portillo, D.G. McLone, T. Tomita, Surgical results of posterior fossa decompression for patients with Chiari I malformation, Childs Nerv. Syst. 20 (5) (2004) 349–356.
[26] P. Brugieres, I. Idy-Peretti, C. Iffenecker, et al., CSF flow measurement in syringomyelia, AJNR Am. J. Neuroradiol. 21 (10) (2000) 1785–1792.
[27] H.S. Chang, H. Nakagawa, Hypothesis on the pathophysiology of syringomyelia based on simulation of cerebrospinal fluid dynamics, J. Neurol. Neurosurg. Psychiatry 74 (3) (2003) 344–347.
[28] R.E. Clatterbuck, E.P. Sipos, The efficient calculation of neurosurgically relevant volumes from computed tomographic scans using Cavalieri's direct estimator, Neurosurgery 40 (1997) 339–343.
[29] S. Aydin, H. Hanimoglu, T. Tanriverdi, E. Yentur, M.Y. Kaynar, Chiari type I malformations in adults: a morphometric analysis of the posterior cranial fossa, Surg. Neurol. 64 (3) (2005) 237–241.
[30] E. Akar, S. Kara, H. Akdemir, A. Kırıs, Fractal dimension analysis of cerebellum in Chiari malformation type I, Comput. Biol. Med. 64 (2015) 179–186.
[31] P. Brugieres, I. Idy-Peretti, C. Iffenecker, et al., CSF flow measurement in syringomyelia, AJNR Am. J. Neuroradiol. 21 (10) (2000) 1785–1792.
[32] H.S. Chang, H. Nakagawa, Hypothesis on the pathophysiology of syringomyelia based on simulation of cerebrospinal fluid dynamics, J. Neurol. Neurosurg. Psychiatry 74 (3) (2003) 344–347.
[33] E.C. Clarke, D.F. Fletcher, M.A. Stoodley, L.E. Bilston, Computational fluid dynamics modelling of cerebrospinal fluid pressure in Chiari malformation and syringomyelia, J. Biomech. 46 (2011) 1801–1809.
[34] T.H. Ha, U. Yoon, K.J. Lee, Y.W. Shin, J.M. Lee, I.Y. Kim, K.S. Ha, S.I. Kim, J.S. Kwon, Fractal dimension of cerebral cortical surface in schizophrenia and obsessive—compulsive disorder, Neurosci. Lett. 384 (2005) 172–176.
[35] F.J. Esteban, J. Sepulcre, N.V. de Mendizábal, J. Goñi, J. Navas, J.R. de Miras, B. Bejarano, J.C. Masdeu, P. Villoslada, Fractal dimension and white matter changes in multiple sclerosis, Neuroimage 36 (2007) 543–549.
[36] Y.T. Wu, K.K. Shyu, C.W. Jao, Z.Y. Wang, B.W. Soong, H.M. Wu, P.S. Wang, Fractal dimension analysis for quantifying cerebellar morphological change of multiple system atrophy of the cerebellar type, Neuroimage 49 (2010) 539–551 (MSA-C).
[37] Z.Y. Shan, J.Z. Liu, J.O. Glassa, A. Gajjarc, C.S. Lid, W.E. Reddicka, Quantitative morphologic evaluation of white matter in survivors of childhood medulloblastoma, Magn. Reson. Imaging 24 (2006) 1015–1022.
[38] S.L. Free, S.M. Sisodiya, M.J. Cook, D.R. Fish, S.D. Shorvon, Three dimension fractal analysis of the white matter surface from magnetic resonance images of the human brain, Cereb. Cortex 6 (1996) 830–836.
[39] J.Z. Liu, L.D. Zhang, G.H. Yue, Fractal dimension in human cerebellum measured by magnetic resonance imaging, Biophys. J. 85 (2003) 4041–4046.
[40] J.M. Lee, U. Yoon, J.J. Kim, I.Y. Kim, D.S. Lee, J.S. Kwon, S.I. Kim, Analysis of the hemispheric asymmetry using fractal dimension of a skeletonized cerebral surface, IEEE Trans. Biomed. Eng. 51 (2004) 1494–1498.
[41] F.J. Esteban, J. Sepulcre, J.R. de Miras, J. Navas, N.V. de Mendizábal, J. Goñi, J.M. Quesada, B. Bejarano, P. Villoslada, Fractal dimension analysis of grey matter in multiple sclerosis, J. Neuro. Sci. 282 (2009) 67–71.
[42] R.D. King, A.T. George, T. Jeon, L.S. Hynan, T.S. Youn, D.N. Kennedy, B. Dickerson, Characterization of atrophic changes in the cerebral cortex using fractal dimensional analysis, Brain Imaging Behav. 3 (2009) 154–166.
[43] P. Tamije Selvy, V. Palanisamy Dr., M. Radhai Sri, A new fuzzy C means for brain image segmentation using anisotropic diffused regularization, IJSETR 1 (November (5)) (2012).
[44] S. Garg, J. Kaur, Improving segmentation by denoising brain MRI images through interpolation median filter in ADTVFCM, Int. J. Comput. Trends Technol. 4–2 (2013).
[45] D.L. Pham, C. Xu, J.L. Prince, Current methods in medical image segmentation, Annu. Rev. Biomed. Eng. 2 (2000) (2000) 315–337.
[46] I. Despotovic, B. Goossens, W. Philips, MRI segmentation of the human brain: challenges, Methods Appl. Comput. Math. Methods Med. 2015 (2015) 23, http://dx.doi.org/10.1155/2015/450341, Article ID 450341.
[47] O. Freifeld, H. Greenspan, J. Goldberger, Lesion detection in noisy MR brain images using constrained GMM and active contours, Proceeding of the 4th IEEE International Symposium on Biomedical Imaging (ISBI 2007) (2007) 596–599.
[48] R. Riji, J. Rajan, J. Sijbers, M.S. Nair, Iterative bilateral filter for Rician noise reduction in MR images, SIViP 9 (7) (2015) 1543–1548, http://dx.doi.org/10.1007/s11760-013-0611-6.
[49] H. Gudbjartsson, S. Patz, The Rician distribution of noisy MRI data, Magn. Reson. Med. 34 (1995) 910–914.
[50] J. Sijbers, A.J. den Dekker, J. Van Audekerke, M. Verhoye, D. Van Dyck, Estimation of the noise in magnitude MR images, Magn. Reson. Imaging 16 (1998) 87–90.
[51] S.O. Rice, Mathematical analysis of random noise, Bell Syst.Tech. J. 23 (1944) 282–332.
[52] S. Basu, et al., Rician Noise Removal in Diffusion Tensor MRI Medical Image Computing and Computer-Assisted Intervention—MICCAI 2006, 4190, LNCS, 2006, pp. 117–125.
[53] C. Koay, et al., Simultaneous identification of noise and estimation of noise standard deviation in MRI, Proc. Int. Soc. Mag. Reson. Med. 17 (2009) 4691 (Honolulu HI).
[54] J. Rajan, D. Poot, J. Juntu, J. Sijbers, Noise measurement from magnitude MRI using local estimates of variance and skewness, Phys. Med. Biol. 55 (2010) N441–N449.
[55] J.W. Tukey, Exploratory Data Analysis (preliminary Ed.). Reading, MA: Addison-Wesley, 1971.
[56] C. Tomasi, R. Manduchi, Bilateral filtering for gray and color images, Proceedings of 6th International Conference on Computer Vision (1998) 839–846.
[57] S.M. Smith, J.M. Brady, Susan—a new approach to low level image processing, Int. J. Comput. Vis. 23 (1997) 45–78.
[58] M. Elad, On the origin of the bilateral filter and ways to improve it, IEEE Trans. Image Process. 11 (2002) 1141–1151.
[59] M. Zhang, B.K. Gunturk, Multiresolution bilateral filtering for Image denoising, IEEE Trans. Image Process. 17 (2008) 2324–2333.
[60] L. Zhang, J.Z. Liu, D. Dean, V. Sahgal, G.H. Yue, A three-dimensional fractal analysis method for quantifying white matter structure in human brain, J. Neurosci. Methods 150 (2006) 242–253.
[61] B.B. Mandelbrot, The Fractal Geometry of Nature, W.H. Freeman, New York, 1983.
[62] M. Nezadal, O. Zmeskal, M. Buchnicek, The box-counting: critical study, Proceedings of the Fourth Conference on Prediction, Synergetic and More 18 (2001) (ISBN 80-7318-030-8).
[63] E. Fernández, H.F. Jelinek, Use of fractal theory in neuroscience: methods, advantages, and potential problems, Methods 24 (2001) 309–321.
[64] G. Ilango, R. Marudhachalam, New hybrid filtering techniques for removal of Gaussian noise from medical images, ARPN J. Eng. Appl. Sci. 6 (2011) 008–012.
[65] J. Jaya, K. Thanushkodi, M. Karnan, Tracking algorithm for de-noising of MR brain images, Int. J. Comput. Sci. Netw. Secur. 9 (2009) 262–267.
[66] S. Patil, V.R. Udupi, Preprocessing To Be Considered For MR and CT Images Containing Tumors, IOSR J. Electr. Electron. Eng. 1 (4) (2012) 54–57.
[67] S. Arastehfar, A.A. Pouyan, A. Jalalian, An enhanced median filter for removing noise from MR images, J. AI Data Mining 1 (1) (2013) 13–17.
[68] E.R. McVeigh, R.M. Henkelman, M.J. Bronskill, Noise and filtration in magnetic resonance imaging, Med. Phys. 12 (1985) 586–591.
[69] G. Gerig, O. Kubler, R. Kikinis, F.A. Jolesz, Nonlinear anisotropic filtering of MRI data, IEEE Trans. Med. Imaging 11 (1992) 221–232.
[70] R.D. Nowak, 1999 Wavelet-based Rician noise removal for magnetic resonance imaging, IEEE Trans. Image Process. 8 (1999) 1408–1419.
[71] P. Bao, L. Zhang, Noise reduction for magnetic resonance images via adaptive multiscale products thresholding, IEEE Trans. Med. Imaging 22 (2003) 1089–1099.
[72] J. Ma, G. Plonka, Combined curvelet shrinkage and nonlinear anisotropic diffusion, IEEE Trans. Image Process. 16 (2007) 2198–2206.
[73] J. Mohan, V. Krishnaveni, Y. Guo, A survey on the magnetic resonance image denoising methods, Biomed. Signal Process. Control 9 (2014) 56–69.
[74] B. Li, D. Que, Medical images denoising based on total variation algorithm, Procedia Environ. Sci. 8 (2011) 227–234.
[75] T.M. Lehmann, C. Gönner, K. Spitzer, Survey: interpolation methods in medical image processing, IEEE Trans. Med. Imaging 18 (11) (1999) 1049–1075.
[76] T. Pant, Effect of noise in estimation of fractal dimension of digital images, Int. J. Signal Processing Image Process. Pattern Recognit. 6 (5) (2013) 101–116.
[77] A.B. Hamza, H. Krim, Image denoising: a nonlinear robust statistical approach, IEEE Trans. Signal Process. 49 (12) (2001) 3045–3054.